Low-Stress Hyperbranched Polymer/Silica Nanostructures Produced by UV-Curing, Sol-Gel Processing and Nanoimprint Lithography

V. Geiser, Y. Leterrier*, J.-A. E. Månson

Laboratoire de Technologie des Composites et Polymères (LTC)

Ecole Polytechnique Fédérale de Lausanne (EPFL)

CH-1015 Lausanne, Switzerland

(*) corresponding author

Abstract

Nanostructured composite materials based on an acrylated hyperbranched polymer (HBP) and up to 25 %vol silica were produced using a combination of sol-gel condensation and photo-polymerization. This dual-cure process was optimized to avoid premature cracking of the sol-gel material. The structure, thermo-mechanical properties and internal stress of the sol-gel composites were compared with particulate nanocomposites processed by solvent-assisted mixing silica nanoparticles with the HBP. All composites were transparent with a homogeneous dispersion of the inorganic phase. The photo-conversion of the HBP was weakly influenced by the presence of silica particles and sol-gel precursors. In all cases the final conversion was independent of UV intensity and a time-intensity superposition for the conversion was observed with power-law dependence of the superposition shift factor on UV intensity. The thermo-mechanically relevant properties of both composites were improved with respect to the polymer matrix (increased Young's modulus and glass transition temperature and decreased coefficient of thermal expansion). The sol-gel composites with a much finer silica network systematically outperformed the particulate composites, including an increase of the glass transition temperature of 63°C and a reduction of the process-induced internal stress by a factor of 2.2 for a silica fraction of 20 vol%. Nano-sized gratings were produced from the sol-gel composites by low-pressure UV-nanoimprint lithography using a glass master. Using an optimal dual-cure sequence enabled the replication fidelity of the composite gratings to be within 97% of the master period for all tested compositions.

Introduction

Polymer nanocomposites are materials of high interest, because the addition of a small amount of inorganic nanoparticles leads to a substantial improvement of the thermo-mechanical properties of the polymer.[1] As examples, 3.4 vol% of copper nanoparticles increased the Young's modulus of low density polyethylene by 29%,[2] and ~5 vol% of aligned carbon nanotubes increased the Young's modulus of polystyrene by 49%.[3] These large increases at low particle fractions are the consequence of the very large specific interfacial area and short distances between the reinforcing particles.[4] The specific surface of spherical particles of radius r and density ρ is equal to $3/(r\,\rho)$, which is of the order of several 100 m^2/g for inorganic particles of radius below 10 nm. The distance between nanoparticles in a suspension rapidly becomes smaller than the particle radius when the particle volume fraction goes beyond a few percent.[5] Further benefits of nanocomposites include a lower polymerization shrinkage with respect to the pure resin[6] and their transparency to visible and UV light, which is especially important if photo-polymerization is used. As a result, nanocomposites are more and more used as photoresists,[7] thermally[8] and UV[9] imprintable resists of dimensionally stable and high precision nanostructures.

A common method to introduce the inorganic phase into the polymer matrix is to mix the monomer or polymer with preformed particles. However, the benefits of nanocomposites rely on a good dispersion of the particles, which is usually associated with processing problems. In fact, small amounts of nanoparticles drastically alter the viscoelastic properties of the material, transforming the liquid-like polymer into a solid-like composite paste. For instance, a 200-fold increase in viscosity was found when ~1.6 vol% fumed silica was added to a cyanate ester,[10] and

the increase was by more than five orders of magnitude when 20 vol% of silica nanoparticles were added to a hyperbranched polymer.[5] The liquid-to-solid transition is a major challenge for nanocomposite processing and is often overcome with the use of solvents.

An alternative route to overcome processing problems of nanocomposites is the use of an organometallic liquid precursor, which forms an inorganic phase in situ in the polymer matrix through sol-gel condensation reactions.[11] Metal alkoxides in the form of $M(OR)_4$, where M is usually Si or Ti and R represents an organic ligand, are popular precursors because they react readily with water. Sol-gel processing was initially only used to produce inorganic monolithic structures or hard films.[12] An issue with sol-gel processes is shrinkage during drying or from evaporation of byproducts, which can be minimized by working without solvents and by minimizing the amount of water engaged in the hydrolysis reaction.[13] Further drawbacks include crack formation in coatings, brittleness of sols or high sintering temperatures necessary for complete densification. These limitations were overcome by adding organic modifiers[14] to the inorganic network to promote the elasticity of the gel. It was shown that only 5% of star alkoxysilane molecules into the inorganic network during sol-gel synthesis substantially increased the toughness, with a Young's modulus within a factor of 2 of that of the inorganic glass. The modified glass showed much higher energy to break and compression strength.[15]

For sol-gel processing of organic/inorganic hybrids an organic monomer and an organometallic precursor are mixed in the liquid state, allowing for a very homogeneous distribution of the reactants on a molecular level as reviewed by several authors.[16, 17] The resulting morphology of the polymerized network is also very homogeneous, with very good dispersions of *in situ* formed

inorganic particles,[11, 13, 16, 18] in particular TiO_2[19, 20] or SiO_2[21] particles. In the latter case, the pH was found to play an important role on the morphology of the forming silica phase. At pH ≤ 2 hydrolysis was faster than condensation, leading to fine silica particles, whereas at higher pH the particles aggregated.[22] The combination of a low pH with the use of a coupling agent enabled very fine silica structures (2-5 nm) intertwined with the polymer network.[23-27] The transformation of the precursor into the metal oxide by hydrolysis and condensation can be performed prior,[26] during[20] or after polymerization.[23] Sol-gel processing has also been used in combination with hyperbranched polymers (HBP), which were found to promote homogeneous networks owing to their multifunctional and spherical nature[20, 28, 29] and UV polymerization.[29, 30]

The objective of the present work was to explore the potential of the sol-gel route to produce hybrid materials based on a liquid organometal precursor and a UV-curable low-shrinkage HBP.[31, 32] A further objective was to evaluate the application of these hybrid materials to the fabrication of nanostructures by a replication method. In fact, composites based on silica nanoparticles and the same UV-curable HBP were successfully applied to nanogratings, using UV-nanoimprint lithography (UVNIL[33]).[34] The functionality of these polymer-based gratings in optical biosensors requiring sub-nanometer dimensional accuracy was further demonstrated.[35] However, some segregation of the nanoparticles occurred due to exudation of the viscous polymer in the tiny grating structure. Moreover, a distortion of the grating geometry was observed when the amount of silica was increased, and this was correlated with the level of internal stress. Particular attention was thus paid in the present work to the thermo-mechanical

properties and internal stress of the sol-gel composites, with respect to composites prepared by solvent-assisted mixing of the HBP with a nanopowder.

Experimental Section

Precursor Materials

The monomer was based on a 3rd generation hyperbranched polyether polyol, giving a 29-functional hyperbranched polyether acrylate (Perstorp AB, Sweden). The photoinitiator was 1-hydroxy-cyclohexyl-phenyl-ketone (Irgacure® 184, Ciba Specialty Chemicals). The organometal precursor was tetraethyl orthosilicate tetraethoxysilane (TEOS, Sigma Aldrich). Methacryloxy(propyl)trimethoxysilane (MEMO, Sigma-Aldrich) was used as a coupling agent to induce covalent bonds between the organic and inorganic phase, and reduce the size of the inorganic domains by pinning the inorganic phase to the matrix, therefore preventing macroscopic phase separation.[36, 37] 1 M HCl in H_2O was purchased from Sigma-Aldrich.

Processing of the Sol-Gel and Particulate Composites

1 wt% of photoinitiator was dissolved in the HBP while stirring at 70°C in an oil bath for 30 min. Following references to HBP will always refer to the mixture of HBP with 1 wt% photoinitiator. The HBP, MEMO, TEOS and 1 M HCl in water were mixed together in this order. After each step the mixture was stirred at room temperature until homogenization was visually observed. After addition of the last compound the mixture was stirred for 30 min. The amount of TEOS was

calculated assuming 100% conversion of the precursor into SiO_2. The amount of coupling agent was calculated to give a concentration of 10% methacrylic groups within acrylic groups. The conversion of the silanol groups into SiO_2 was also assumed to be 100%. The amount of H_2O was calculated to give a molar ratio of H_2O to ethyl groups equal to 1:2. Condensation of the inorganic phase was done at 80°C for 4 h. The density of the resulting silica phase was assumed to be equal to 2 g/cm^3. Photo-polymerization of the HBP network was done using a UV intensity of 50 mW/cm^2 either before, after or during the condensation process, as detailed in the Results and Discussion Section. The sol-gel composites were cured in the form of 100 to 400 μm thick films.

The sol-gel composites were compared with particulate composites containing the same amount of silica. These particulate composites were based on the same acrylated HBP mixed with 13 nm silica organosol particles of density equal to 2.11 g/cm^3 (HL, Highlink® NanO G502, Clariant), as detailed in a recent work.[32] Particle suspensions in isopropanol were mixed with the HBP and stirred for 30 min at room temperature. The solvent was removed at 40°C under vacuum until no more weight change was recorded. Films of 100 – 400 μm in thickness were subsequently photo-polymerized at 50 mW/cm^2.

A UV lamp with a 200 W high-pressure mercury bulb (OmniCure 2000, Exfo, Canada) in combination with a liquid light guide was used for all experiments. The light intensity on the sample was measured using a spectrometer (Sola-Check, Solatell, UK) over the range of 270 to 470 nm.

Methods

The kinetics of the photo-polymerization reaction was analyzed by means of photo-differential scanning calorimetry (photo-DSC, Q100 TA Instruments) to investigate the influence of the sol-gel precursor and silica particles on the conversion of the acrylated HBP. The calorimeter cell was equipped with a light guide accessory and was sealed with a quartz window that let the UV light pass onto the open aluminum sample pans. Neutral filters were used for experiments at low UV intensity. Measurements were carried out at room temperature. The residual temperature increase of the sample, due to the irradiation from the lamp, was less than 1°C. The heat of polymerization was recorded as a function of time and the double bond conversion x was calculated according to Hoyle[38] from the total heat of reaction calculated by integrating the exothermic peak:

$$x = \frac{H_{HBP}}{H_{100\%}} = \frac{H_{total}/m_{HBP}}{[AG]\cdot\Delta H_{AG}} \tag{1}$$

where H_{HBP} is the heat of reaction per gram of HBP, H_{total} is the measured heat of reaction per gram of sample, $H_{100\%}$ is the theoretical heat for 100% double bond conversion of the HBP, m_{HBP} is the weight fraction of HBP, $[AG]$ is the concentration of acrylate groups in the HBP and ΔH_{AG} is the energy of the acrylate double bond equal to 86.31 kJ/mol.[39] Equation (1) is valid for the conversion of HBP in the particulate composites. For the sol-gel composites the heat of reaction of the methacrylate groups of the coupling agent equal to 54.89 kJ/mol[39] was also taken into account, assuming that all methacrylate groups reacted during the photo-polymerization reaction.

The condensation of the inorganic phase was measured by solid-state ^{29}Si-NMR (Avance 400, Bruker). The spectra were obtained at 59.62 MHz and the solid samples were ground prior to analysis. NMR spectra were deconvoluted using Gaussian fits in terms of Q_i where $i = 2, 3, 4$ correspond to the number of siloxane bridges bonded to the silicon atom of interest. The condensation state Ω was calculated according to:[25]

$$\Omega = \sum_{i=2}^{4} \frac{i}{4} Q_i = \frac{1}{2} Q_2 + \frac{3}{4} Q_3 + Q_4 \tag{2}$$

The viscosity of the unpolymerized materials at room temperature was measured using a strain-controlled rotational rheometer (ARES, Rheometrics Scientific). This information is essential for process optimization, especially in the case of nano-imprinting. Due to the low viscosity of the mixtures containing the sol-gel precursor, measurements were done with a Couette geometry using a cylinder diameter of 25 mm, cylinder length of 32 cm and wall space of 1 mm. For the particulate composites a cone-plate geometry with a diameter of 25 mm, a cone angle of 0.1 rad and a gap of 0.051 mm was used. The strain was ensured to be in the linear viscoelastic range at any frequency.

The microstructure of the two types of composites was investigated by TEM (Philips/FEI, CM20 at 200 kV). The samples were embedded in an epoxy resin (Epoxy resin medium kit, Fluka) and cut with a diamond knife on a microtome (Ultracut E, Reichert-Jung) to 40 nm thick slices, then put on a carbon-coated grid.

Three methods were used to characterize the thermo-mechanical properties of the materials (glass transition temperature, Young's modulus and coefficient of thermal expansion) since these properties determine the stability of small-scale polymer-based structures.

The glass transition temperature T_g of the HBP and composites was determined by means of differential scanning calorimetry (DSC, Q100, TA Instruments) at a heating rate of 10 K/min between -20°C and +100°C.

The tensile modulus and the transition temperature of the HBP and composites were measured in a dynamic mechanical analyzer (DMA, Q800, TA Instruments) under axial oscillatory deformation at a frequency of 1 Hz and maximum strain of 0.15% during heating from room temperature up to 150°C at a rate of 10 K/min.

The coefficient of thermal expansion (CTE) of the HBP and composites was measured with a thermo-mechanical analyzer (TMA 402, Netsch) using a heating and cooling rate of 5 K/min.

Internal stresses represent a key problem in terms of dimensional stability of polymer micro- and nano-structures and as previously pointed out an objective was to determine the possible benefits of the combination of UV curable HBP and sol-gel precursor towards stress reduction. The in-plane internal stress σ_i of the HBP and composite films was determined from the curvature of coated aluminum beams as detailed in the work of Schmidt et al.,[31] and calculated according to the model of Inoue:[40]

$$\sigma_i = -\frac{E_s h_s^2}{6 r h_c}\left(\frac{\left(1-uq^2\right)^3\left(1-u\right)+\left(uq(q+2)+1\right)^3+u\left(uq^2+2q+1\right)^3}{2\left(1+q\right)\left(1+uq\right)^3}\right) \text{ with } u=\frac{E_c}{E_s} \text{ and } q=\frac{h_c}{h_s} \qquad (3)$$

where E_s and E_c are the moduli of the substrate and the coating, respectively, h_s and h_c are the corresponding thicknesses and r is the radius of curvature.

The SiO$_2$ weight content and thermal stability of the composite materials were measured in a thermo-gravimetric analyzer (TGA, SDTA851^e, Mettler Toledo), in an oxygen environment. The composites were cured in the form of approximately 100 μm thick films and then broken down to small pieces of a few square mm and mass between 18 and 29 mg. The weight loss was recorded while the samples were heated from ambient temperature to 800°C at 10 K/min.

UV-Nanoimprint Lithography

Nanogratings were produced using a UVNIL tool that was designed in-house as detailed in a previous publication.[34] The master was a dry etched glass grating with a period of 364 ± 5 nm and a step height of 12 ± 1 nm. This particular grating structure is used in wavelength-interrogated optical sensors (WIOS) developed for immunoassay purposes [41]. The material to imprint was dispensed on the master and covered with a glass slide, the surface of which was treated with methacrylsilane to improve adhesion. A pressure of 6 bars was applied while the material was polymerized through the quartz window. Approximately 12% of UV light was absorbed through the glass carrier. The UV intensities reported in the Results Section were measured under the glass carrier, i.e. on the sample surface. After polymerization the pressure

was released and the master was removed from the imprinted material attached to the glass

carrier. No special surface treatment was needed to help demolding, due to the 25° clearance

angle of the glass grating. The topography of the gratings was analyzed by atomic force

microscopy (AFM, Multimode II, Veeco) in contact mode using a tip with a spring constant of

0.06 N/m. A total of 512 scans were recorded over a length of 2 μm, and were averaged to give

the grating profiles shown in Figure 11.

Results and Discussion

Process – Microstructure Relations

The sol-gel composites were produced using a "dual-cure" photo-polymerization and

condensation process. Photo-polymerization was carried out either before, after, or at a specific

time (referred to as t_{UV} in the following) during the condensation. In all cases, condensation lasted

in total 4 h. When photo-polymerization was done before condensation ($t_{UV} = 0$), the low

viscosity of the HBP/precursor mixture facilitated processability. However high shrinkage

occurred during subsequent condensation due to the evaporation of byproducts, and the stress

was released through cracking of the composite. When photo-polymerization was done after

completed condensation reaction ($t_{UV} = 240$ min), evaporation shrinkage occurred in the liquid

material and no shrinkage stress built up. This process, however, greatly compromised the

processability of the composite, due to the increased viscosity of the material when the silica

network was formed. To benefit from the low viscosity for processing without cracking of the

polymerized material, an optimal sequence for the two processes was found, where photo-

polymerization was done some time after the condensation reaction had started. A certain amount of byproduct could thus evaporate before a rigid network was formed and the shrinkage stress could relax in the still liquid polymer.

For all investigated t_{UV} values, the sol-gel composites remained completely transparent, as did the particulate composites. Figure 1 shows TEM micrographs of the two types of nanocomposites with 5 and 20 vol% of silica (the sol-gel composites were produced using $t_{UV} = 240$ min and their actual amount of silica was equal to 4.5 vol% and 19.3 vol%, respectively, as detailed in the following). A homogeneous dispersion of monodispersed SiO_2 particles is visible for the particulate composites, while for the sol-gel composites no phase contrast can be seen (even using defocusing for contrast enhancement). This was presumably due to a very fine silica network promoted by the coupling agent that copolymerized with the HBP network and prevented macroscopic phase separation of the forming silica, as was found in another work.[23]
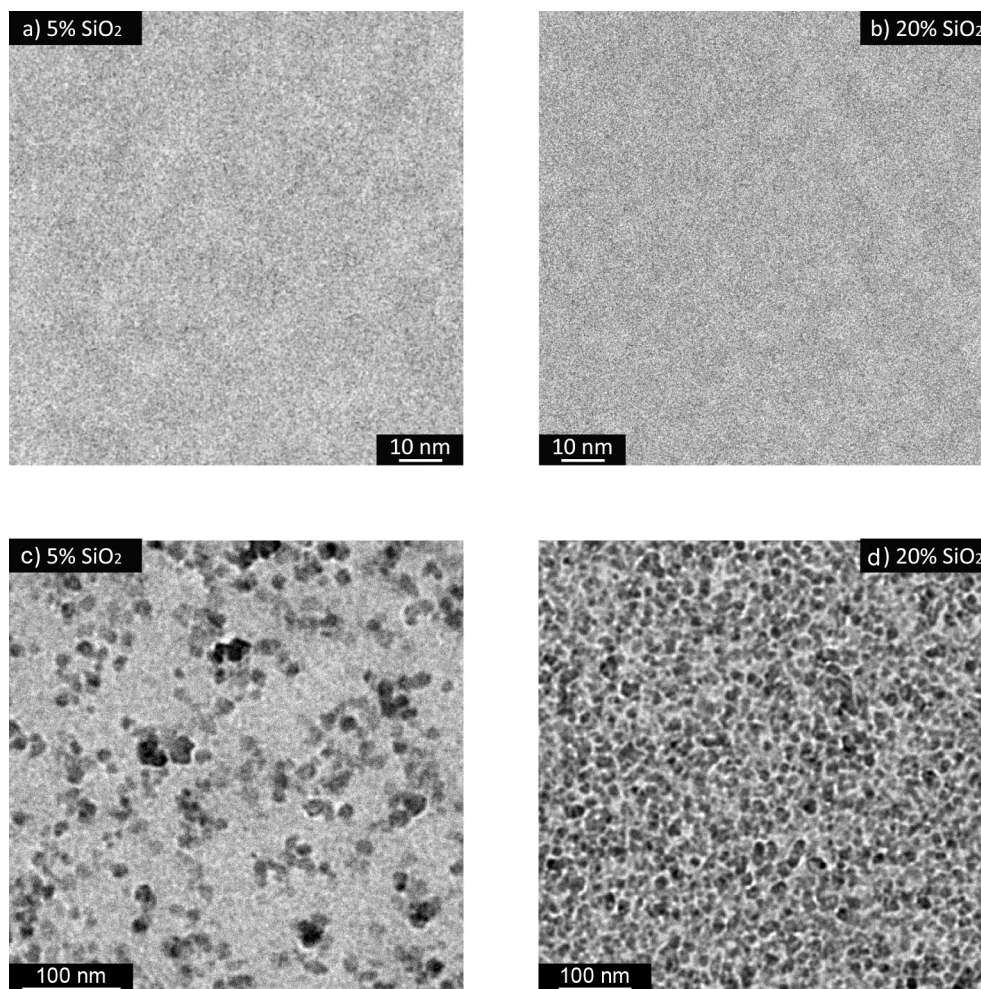
Figure 1. Transmission electron micrographs of the sol-gel composites produced using t_{UV} = 240 min at 5 vol% (a) and 20 vol% (b) silica and particulate composites at 5 vol% (c) and 20 vol% (d) silica.

The photo-polymerization kinetics of the acrylate groups of the HBP in presence of sol-gel precursors or silica particles were investigated with attention paid to the influence of the UV light intensity. The final conversion of the HBP was equal to 74±1% and increased to 83±0.5% with the highest amount of precursor investigated, whereas it decreased to 65±1% in presence of 20 vol% of silica particles. A similar finding was reported by Li et al.[26] when other studies[23, 29] showed that the presence of TEOS as a sol-gel precursor did not influence the final conversion, but in some cases increased the rate of reaction. At low precursor level the reduced viscosity and

hence increased mobility of the radicals presumably provoked the increase in conversion rate and conversion. It was assumed that at higher precursor level the dilution of the reacting species became more important and led to the opposite trend in conversion rate.

An autocatalytic model was used to analyze the conversion data of the HBP and composites.[42] The same reaction order equal to 1.9±0.1 and same autocatalytic exponent equal to 0.7±0.2 were found for all three types of materials and all compositions. For both sol-gel and particulate composites the final conversion was moreover independent of UV intensity. This result is contradictory to the results reported by Schmidt *et al.*[43] and Lecamp *et al.*[44] who found that conversion increased at higher intensities. The reason is in fact due to the different choices of limits for the integration of the heat flow with time. In the present case, the DSC peak was integrated from the time the lamp was switched on until the time when there was no longer any measurable change in the heat flow by DSC, whereas Schmidt defined the conversion reaction to be completed, when the heat flow reached 1/100th of its maximum value.[45] By choosing the same integration criteria as Schmidt, the influence of the intensity on the maximum conversion also became apparent.

A time-intensity superposition behavior was moreover observed for the present HBP-based materials:

$$x\left(t_1, I_1\right) = x\left(t_0, I_0\right) \Leftrightarrow t_1 = \frac{t_0}{a_I} \qquad (4)$$

where x is the conversion, t is the time, I is the irradiation intensity and a_I is the time-intensity

shift factor. The validity of this approach was demonstrated by Corcione *et al.*[46] and Dalle

Vacche et al.[47] for the photo-polymerization of non-vitrifying epoxy-based resin and acrylated

nanocomposites, respectively. Figure 2 shows the shift factors determined using the data at a

reference intensity equal to 0.5 mW/cm^2 for the HBP and the two types of composites. A power-

law dependence of the shift factor on the intensity $a_I = a_0 \cdot I^b$ where a_0 is a proportionality factor

and b is the exponent is evident. The power-law exponents b of all materials are given in the

figure. They are close to each other with an average equal to 0.68±0.04. These results show that

the termination mechanism[42] of the acrylate double bonds was weakly influenced by either the

silanol surface of the silica particles or by the methacrylate coupling agent.
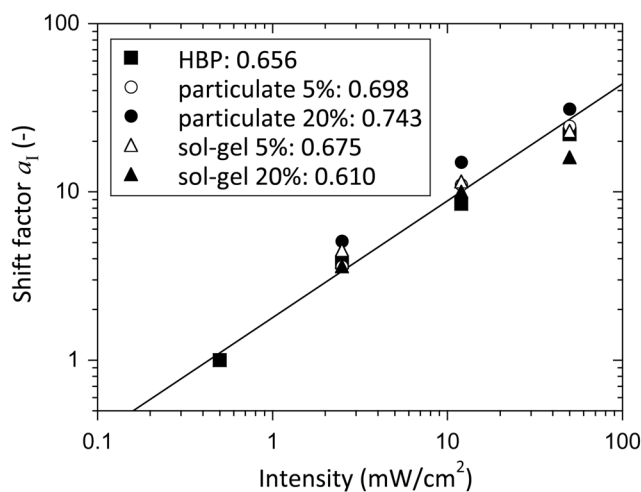

Figure 2. Time-intensity shift factor for HBP, particulate composites and sol-gel composites at 5 %vol and 20 %vol fraction of silica as indicated. The power-law exponents for each material are also indicated and the solid line represents the average power-law fit to the data.

Thermo-gravimetric analysis confirmed the presence of a non-volatile phase in the HBP and the

composites. In the case of pure HBP the residue was a black powder (probably carbon char).

Non-volatile residues were also found in epoxy resins, where carbon char contents up to 8% were

recorded.[29] In the case of the composites the residue was a fine white powder, the amount of

which was close to the theoretical amount of silica, if the HBP residue was subtracted (Figure 3
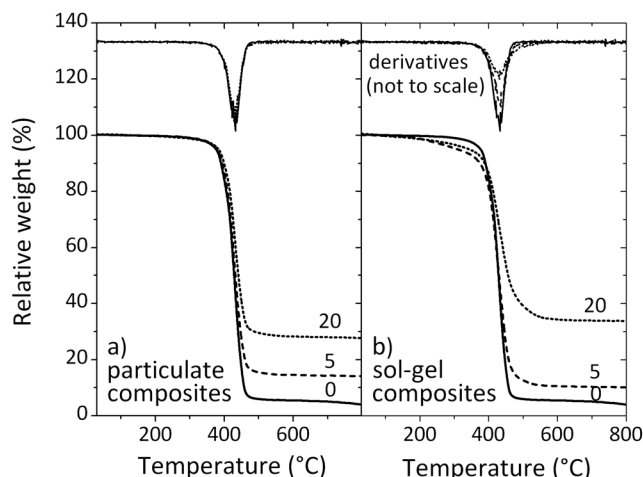
and summarized in Table 1).

Figure 3. Relative weight and derivatives as a function of temperature for the particulate (a) and the sol-gel composites produced using t_{UV} = 240 min (b) with different silica fractions (vol% as indicated).

The presence of a silica phase was further confirmed by solid state ^{29}Si-NMR (Figure 4). The

deconvoluted spectra gave signals at approximately -92, -102 and -113 ppm. The position of the

peaks was close to those described in other studies and corresponded to Q_2, Q_3 and Q_4 species,

respectively.[25, 48] The condensation state Ω of the sol-gel silica was calculated using Equation

(2) and found to be equal to 84%, with a majority of Q_4 species, which compares with the value

of 89% for the Highlink organosol particles.[25] The lower condensation state for the sol-gel silica

was presumably due to the presence of the coupling agent, which can form maximum three Si-O

bonds corresponding to the Q_3 state.

Table 1. Non-volatile residue and silica fraction of sol-gel composites.

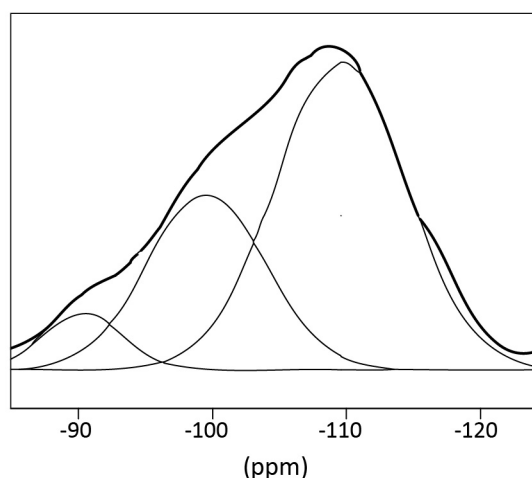|			
Theoretical volume fraction of inorganic phase, ϕ (%)	0	5	20
Theoretical weight fraction of inorganic phase (%)	0	8.7	31.1
Measured weight residue (%)	1.5	10.2	33.8
Calculated volume fraction of inorganic phase (%)	0	4.5	19.3

Figure 4. ^{29}Si-NMR data and deconvoluted peaks of a sol-gel composite produced using t_{UV} = 240 min with 20 vol% of inorganic phase.

Thermo-Mechanical Properties

As shown in Figure 3 the polymerized HBP network was stable up to approximately 400°C, above which thermal degradation occurred in one step (one single derivation peak). The thermal stability of the particulate composites was only marginally improved with the addition of SiO_2. For the sol-gel composites, the weight loss which became detectable below 400°C was presumably due to evaporation of trapped side products or finalization of incomplete condensation.[23, 24] The more distinct weight loss at $T \approx 400$°C, corresponding to the degradation

of the polymer network, occurred at the same temperature as for the pure HBP. This is contradictory to the results of Amerio et al.,[37] who found the degradation of the network to occur at higher temperatures for sol-gel composites with increasing silica content, which they attributed to the formation of an oxygen barrier layer of char.

The glass transition temperature as determined from calorimetric experiments, $T_{g,DSC}$, was around 9°C for the HBP and the particulate composites (Figure 5), i.e. the silica particles did not influence the glass transition behavior of the HBP. For the sol-gel composites the $T_{g,DSC}$ could not be determined, since no step in the heat capacity was observed. Such a behavior is generally related to complete immobilization of the polymer matrix by the inorganic phase,[49] and supports the earlier assumption of the silica being in the form of a fine network structure with very high specific surface area.
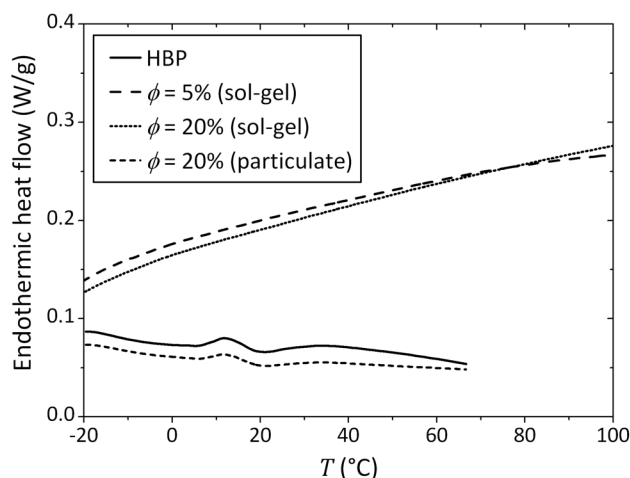

Figure 5. Endothermic heat flow during heating for HBP, particulate composites with 20 vol% of silica and sol-gel composites produced using t_{UV} = 240 min with 5 and 20 vol% of silica.

Figure 6 displays the storage modulus and tangent of the phase angle δ of the polymer and the two types of composites with 20 vol% of silica. In all cases a broad glass transition is evident, which reflects the broad distribution of relaxation times in hyperbranched molecular architectures.[50] The behavior of the particulate composite is similar to that of the HBP, with comparable amplitude of the tan δ peak. The amplitude of the peak is however significantly lower for the sol-gel composite, and the transition is even broader (data lacking above 150°C). It is moreover clear that the modulus and glass transition temperature (defined as the peak temperature on tan δ) of both composites are higher compared to the HBP. The glass transition temperature determined from dynamic mechanical analysis, $T_{g,DMA}$, increased with the filler fraction for both types of composites (inset in Figure 6). At $\phi = 20\%$ the $T_{g,DMA}$ of the sol-gel composites was equal to 127°C, which was considerably higher than that of the particulate composites at 69°C. Hence, mechanical stability is given up to significantly higher temperatures for the sol-gel composites.
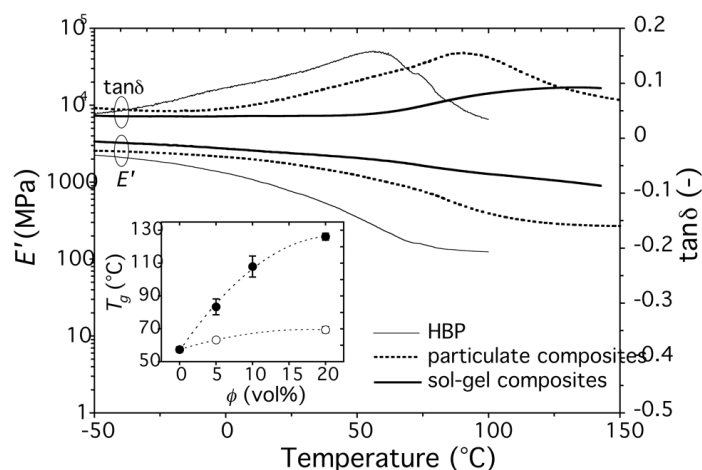

Figure 6. Storage modulus E' and tangent of the phase angle δ as a function of temperature for HBP and composites with 20 vol% of silica. The inset shows the glass transition temperature T_g of the particulate and sol-gel composites as a function of silica fraction ϕ. The sol-gel composites were produced using t_{UV} = 240 min. The dotted lines in the inset are guides for the eye.

Figure 7 shows the dynamic moduli E^* for the particulate and the sol-gel composites. In the latter case the "Condensation first" process ($t_{UV} = 240$ min) was chosen, but the processing sequence for the sol-gel composites only had a minor influence on the values of E^*, as is demonstrated in Figure 8. For both types of composites the modulus was proportional to the filler fraction, and it was 50% higher in the case of the sol-gel composites. This strengthens the assumption that the inorganic phase was in the form of a fine 3-dimensional silica network, which was able to immobilize the surrounding polymer more effectively than the discrete particles.
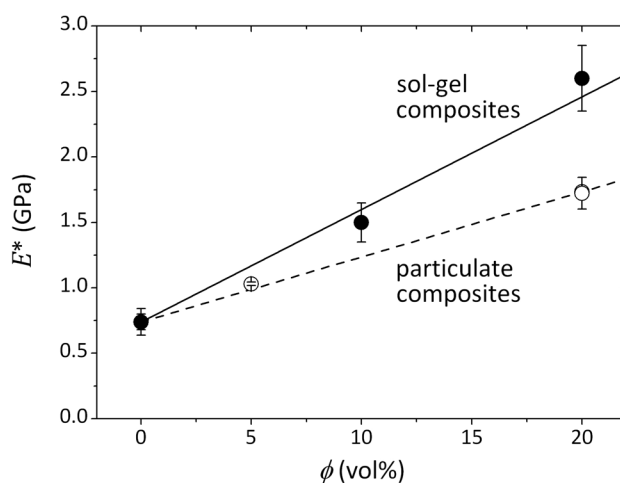

Figure 7. Dynamic modulus E* of particulate and sol-gel composites as a function of silica fraction ϕ. The sol-gel composites were produced using t$_{UV}$ = 240 min. The lines are guides for the eye.
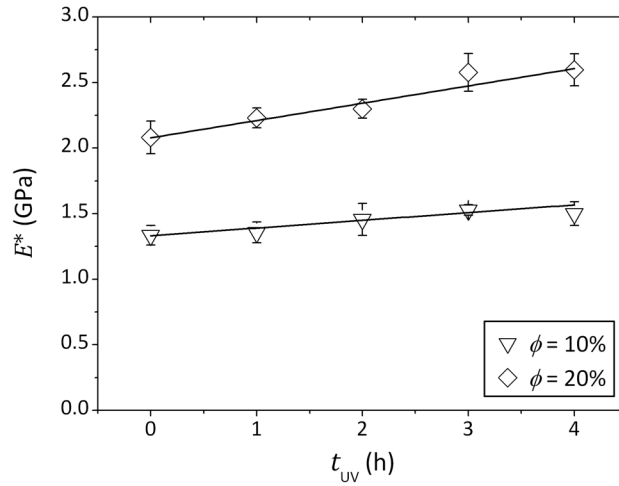
Figure 8. Dynamic modulus E* of sol-gel composites at 10% and 20% volume fractions of silica, photo-polymerized after different condensation periods t$_{UV}$. The lines are guides for the eye.

The coefficient of thermal expansion (CTE) decreased with increasing amount of silica (Figure 9). It was 25% lower for the sol-gel composites compared with the particulate composites at $\phi = 20\%$. For both types of composites the decrease of the CTE with the volume fraction of silica ϕ could be described by the empirical Thomas model:

$$\alpha_c^{\upsilon} = \phi \cdot \alpha_{SiO2}^{\upsilon} + \left(1 - \phi\right) \cdot \alpha_{HBP}^{\upsilon} \tag{5}$$

where α_c, α_{SiO2} and α_{HBP} are the CTE of the composite, inorganic silica phase and HBP phase, respectively, and the fitted exponent υ was equal to 0.7 and 0.27 for the particulate and the sol-gel composites, respectively. The value of α_{SiO2} was taken from literature data for fused silica (5 10^{-7} K^{-1}).
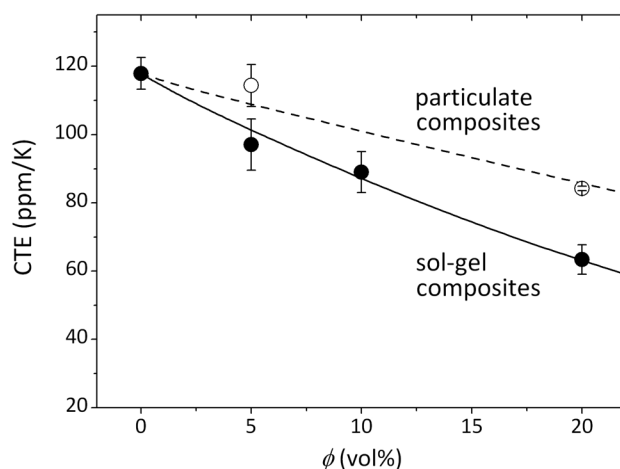
Figure 9. Coefficient of thermal expansion of particulate and sol-gel composites. The sol-gel composites were produced using t_{UV} = 240 min. The lines represent Equation (5) with adjustable exponent υ.

To summarize, all thermo-mechanical properties were improved with the addition of silica (increased Young's modulus and glass transition temperature and decreased coefficient of thermal expansion), and the improvement was more pronounced for the sol-gel composites. This was presumably due to the very fine silica structure, leading to a higher specific HBP/SiO$_2$ interfacial area than in the particulate composites.

Internal Stress

Figure 10 shows the process-induced internal stress of the particulate and sol-gel composites. The internal stress of the former increased linearly with the filler fraction, from 1.3 MPa for the pure HBP to 5 MPa for the composite with 20 vol% of silica particles, in spite of a reduced conversion of the acrylated HBP. This was due to the increased stiffness of the material (Figure 7), which outplayed the 33% reduction of polymerization shrinkage of the HBP upon addition of silica.[32] A remarkably different behavior was found for the sol-gel composites, for which the stress was

independent of the inorganic fraction within experimental scatter. This result was unexpected since the conversion of the HBP was found to increase with the amount of sol-gel precursor. The increase of the stress from $\phi = 0$ to 5% was the same as that of the particulate composite. However at $\phi > 5\%$ considerably less stress developed in the sol-gel composites and, at $\phi = 20\%$, the stress was a factor of 2.2 lower compared to the particulate composites.
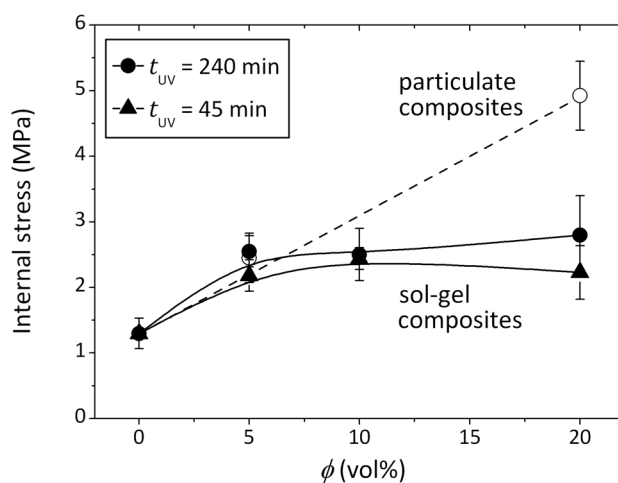

Figure 10. Process-induced internal stress of particulate and sol-gel composites as a function of silica fraction ϕ and condensation time before photo-polymerization, t_{UV}. The lines are guides for the eye.

The process sequence did not change the internal stress either, apart from the "UV-first" case ($t_{UV} = 0$), for which samples cracked during condensation and their internal stress could not be measured. Cracking did not occur for t_{UV} of 45 min and 240 min and in these cases the stress level was the same. In the case of $t_{UV} = 45$ min the precursor was only partially transformed into SiO_2 at the onset of photo-polymerization. The inorganic phase was not yet in the form of a rigid network and the HBP was still swollen (i.e. plasticized) with the liquid precursor. Therefore, polymerization shrinkage occurred in a rather soft material, which favored relaxation of the

shrinkage stress. For the "condensation first" case (t_{UV} = 240 min), the precursor was completely transformed into a rigid SiO_2 network and the byproducts were evaporated before photo-polymerization. The present finding of a considerable stress reduction compared to the particulate composites was thus not expected. It may result from a reduced polymerization shrinkage, which was not measured for these materials due to evaporation phenomena. As the silica was in the form of a fine inorganic network, shrinkage of the intertwined polymer was presumably restricted by the rigid inorganic network structure.

Table 2 recapitulates the properties of the two types of HBP nanocomposites. Clearly, the sol-gel composites are far less viscous, their Young's modulus and glass transition temperature are significantly higher, and their coefficient of thermal expansion and internal stress are much lower than the particulate composites. This combination of properties should be beneficial to produce nanostructures with very high stability.

Table 2. Comparison of pure HBP, sol-gel composites (produced using t_{UV} = 240 min) and particulate composites with 20 %vol silica fraction. Values were taken at room temperature, where applicable.

Process method	η	E^*	CTE	$T_{g,DMA}$	σ_i
	(Pa·s)	(GPa)	(10^{-6} K^{-1})	(°C)	(MPa)
Pure HBP	4.6	0.7	118	58	1.3
Sol-gel condensation with TEOS	$1.3 \cdot 10^{-2}$	2.6	63	127	2.2
Mixing with silica nanoparticles	$2 \cdot 10^5$	1.7	84	69	4.9

UV-Nanoimprint Lithography of Sol-Gel Composites

The production of dimensionally stable nanostructures based on the particulate composites by UVNIL was already demonstrated.[34] The 360 nm period of the glass grating was replicated in the composite material with accuracy better than 98%, even at high loading of nanoparticles. However, a distortion of the grating geometry was observed when the amount of silica was increased, which was correlated with the increasing amount of internal stress.

The sol-gel gratings were produced in a similar way as the particulate composite gratings, the main difference being the additional condensation. The HBP solution placed on a glass carrier was first allowed to condensate for a time t_{UV}, and then was loaded in the UVNIL tool, where it was pressed onto the master using a transparent quartz tool. The sample was illuminated with UV light under a constant pressure of 6 bars for 5 min, and the cured material was put back in the condensation oven.

Figure 11 compares the geometry of the glass master and sol-gel composite gratings with 25 %vol of silica produced using different t_{UV} values. The troughs in the corners of the glass grating resulted from the dry etching step, and were reproduced in the composite gratings. The "UV first" process systematically led to excessive deformation and cracking of the sample during condensation. The resulting nanogratings could therefore not be analyzed and were unsuitable for the application to optical devices. No such problems occurred when photo-polymerization was delayed with respect to the start of the condensation. Stable gratings with high replication fidelity were produced with a t_{UV} of 45 min. The replication fidelity however degraded with increasing

t_{UV} due to the rapid increase of viscosity of the drying material, and the grating was barely detectable when photo-polymerization was done after completion of the condensation (t_{UV} = 240 min).

Figures 12 and 13 show the grating dimensions measured using the AFM profiles. The grating period was nearly preserved with fidelity better than 97% for all investigated compositions and process sequences (Figure 12). However, as shown in Figure 13a, the step height of nanocomposites with 25 vol% of silica progressively degraded and almost completely disappeared when the condensation time before photo-polymerization increased. The reason was that the pressure (6 bars) was insufficient to imprint the rigid silica network. The top and bottom dimensions did not markedly change with t_{UV}, but in fact were approximately 50% larger and 50% smaller, respectively, than that of the master. Such a distortion of the imprinted grating does not compromise its optical performance, controlled by the period and the step height.[34] It was attributed to the relaxation of the internal stresses generated during processing upon release from the master.[34] Figure 13b shows the dimensions of the sol-gel gratings with different silica fractions and for t_{UV} = 45 min. The step height was almost identical to that of the master for all investigated compositions, and a similar distortion of the top and bottom dimensions as previously noticed in Figure 13a was also evident. This result confirms the previous finding that the distortion was correlated to the internal stress level,[34] found in the present study to be independent of composition (Figure 10).
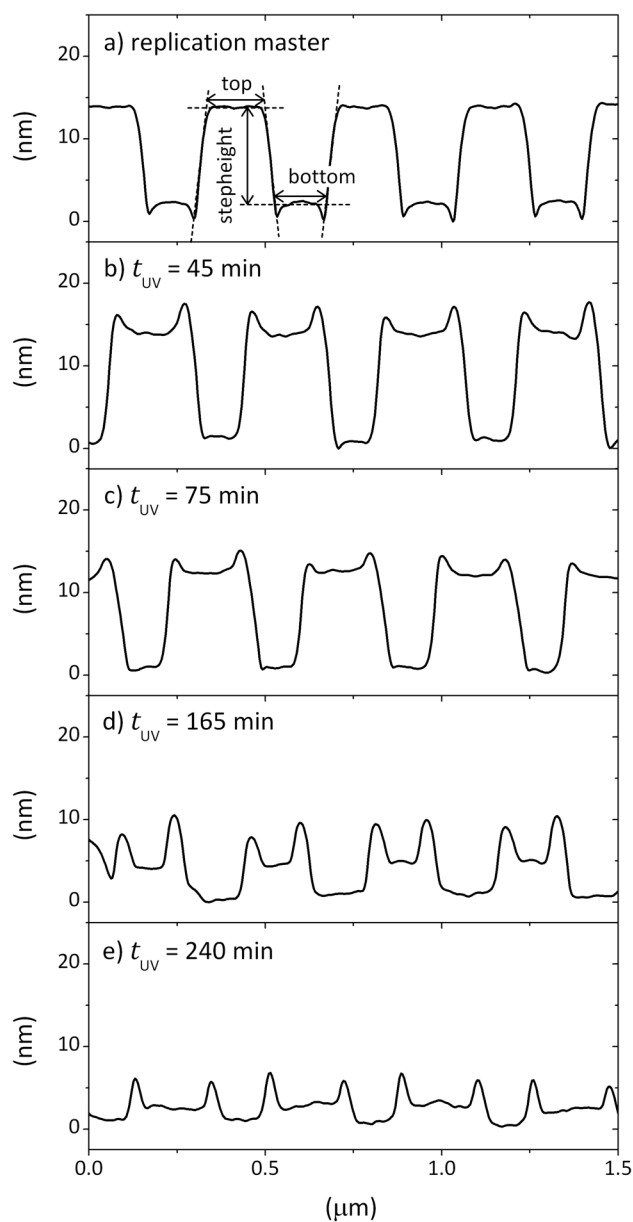
Figure 11. Averaged AFM profiles of the glass master grating with relevant dimensions (top, bottom and step height, a) and sol-gel composite gratings at $\phi = 25\%$ with photo-polymerization done after different condensation periods t_{UV} as indicated on the graphs (b-e). In all cases the total condensation time was 240 min and the photo-polymerization parameters were $I = 50$ mW/cm^2, $p = 6$ bars, $t = 300$ s.
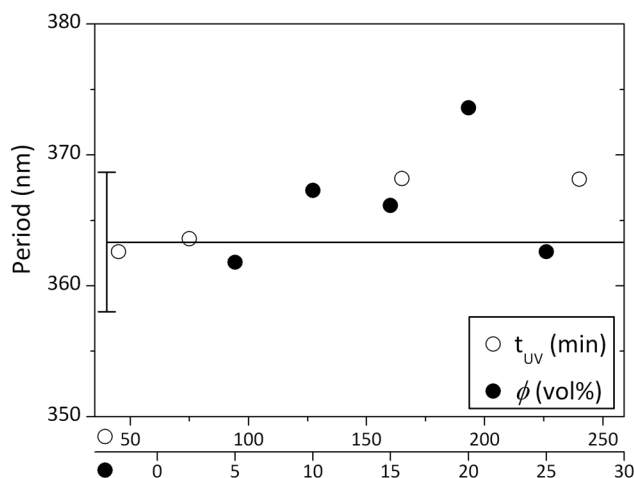
Figure 12. Grating period as a function of condensation time before photo-polymerization t_{UV} at $\phi = 25\%$ (open symbols), and as a function of filler fraction for $t_{UV} = 45$ min (closed symbols). The line with the error bar represents the period of the replication master. The total condensation time was 240 min and the photo-polymerization parameters were $I = 50$ mW/cm^2, $p = 6$ bars, $t = 300$ s.

To summarize, the timing of the photo-polymerization reaction with respect to the condensation reaction was critical to achieve accurate sol-gel composite nanostructures. The optimal process sequence (45 min of condensation prior to UV illumination) enabled to relax most of the evaporation shrinkage stress while ensuring a sufficiently soft silica network, which could be imprinted with a very high fidelity at a low pressure.
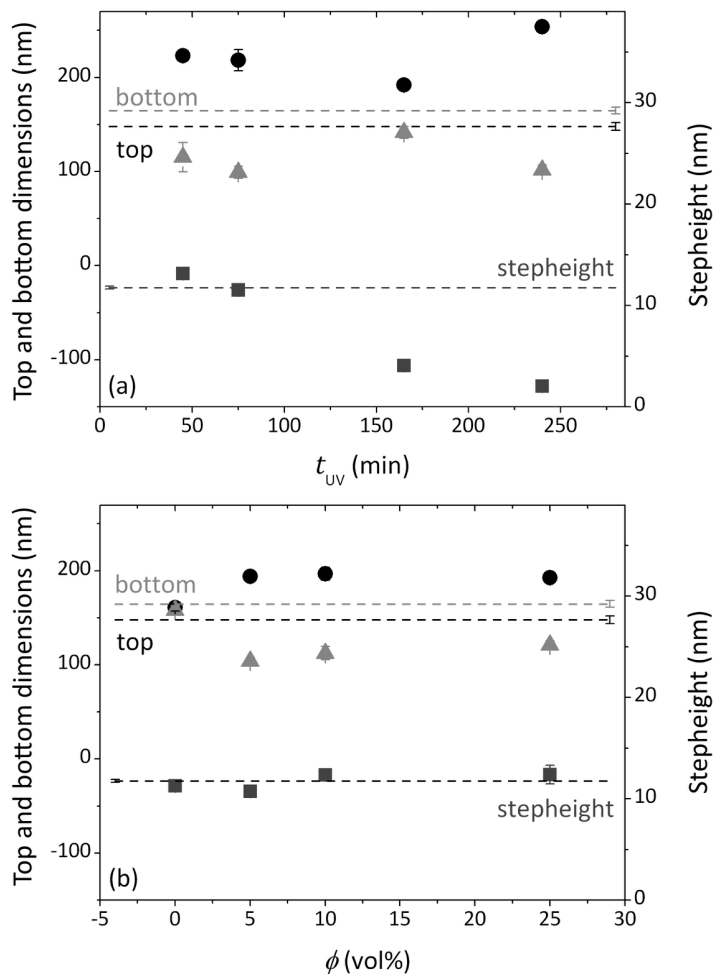
Figure 13. Grating dimensions for sol-gel nanocomposites as a function of (a) the duration of the initial condensation period before photo-polymerization at a silica fraction ϕ = 25 % and (b) the volume fraction of silica with photo-polymerization done after 45 min of condensation. The dotted lines represent the dimensions of the glass grating (top, bottom and step height as indicated). Circular symbols: top dimension; triangular symbols: bottom dimension; square symbols: step height. The total condensation time was 240 min and the photo-polymerization parameters were I = 50 mW/cm², p = 6 bars, t = 300 s.

Conclusions

Hybrid HBP/silica nanocomposites were prepared using a dual-cure process based on an *in situ* sol-gel method and photo-polymerization, and their properties were compared with particulate nanocomposites obtained using a solvent assisted mixing process. The dual-cure process sequence was optimized to avoid premature cracking of the sol-gel material due to excess evaporation. A homogeneous dispersion of the inorganic phase was achieved for both types of composites and all investigated compositions were transparent. The photo-conversion process of the acrylate groups of the HBP was weakly influenced by the presence of silica particles and sol-gel precursors. In all cases the final conversion was independent of UV intensity and a time-intensity superposition for the conversion was observed with power-law dependence of the superposition shift factor on UV intensity.

The Young's modulus and glass transition temperature of both types of composites were significantly higher, and their coefficient of thermal expansion was lower than that of the pure HBP. The sol-gel composites systematically outperformed the particulate composites. At a silica fraction of 20 vol% the stiffness of the sol-gel composites was a factor of 3.5 higher than that of the HBP, the glass transition temperature was increased by 63°C and the coefficient of thermal expansion was reduced by 46%. In addition, the process-induced internal stress of sol-gel composites with 20 vol% of silica was a factor of 2.2 smaller compared to the particulate counterpart. These improved properties of the sol-gel materials were attributed to the much finer silica network with higher specific surface area compared to the nanoparticle analogue.

Nano-sized gratings were produced from the sol-gel composites with up to 25 vol% silica by UVNIL in a low-pressure process using a glass master. The period of the composite gratings was within 97% of the master period for all tested compositions. However, the lateral dimensions of the grating deformed by up to 50% for $\phi \geq 5\%$ due to increased internal stress. The highest fidelity was achieved with 45 min of condensation at 80°C, followed by 5 min of photo-polymerization under 50 mW/cm^2, and then completion of the condensation reaction for an additional 195 min at 80°C. In spite of much longer cycle times due to the condensation step, the present low viscosity sol-gel composites offer improved processability, higher stiffness and glass transition temperature, and lower coefficient of thermal expansion and internal stress compared to particulate composites.

Acknowledgements

References

1.   M. Pluta, A. Galeski, M. Alexandre, M. A. Paul, P. Dubois, *J. Appl. Polym. Sci.* **2002**, *86*, 1497-1506.

2.   X. P. Xia, C. S. Xie, S. Z. Cai, F. Wen, C. H. Zhu, X. L. Yang, *Mater. Sci. Eng. A-Struct.* **2006**, *429*, 329-333.

3.   E. T. Thostenson, T.-W. Chou, *J. Phys. D Appl. Phys.* **2002**, *35*, L77-L80.

4.   A. Tewari, A. M. Gokhale, *Mater. Sci. Eng. A-Struct.* **2004**, *385*, 332-341.

5.   V. Geiser, Y. Leterrier, J.-A. E. Månson, *Macromolecules* **2010**, *43*, 7705-7712.

6.   M. Atai, D. C. Watts, *Dent. Mater.* **2006**, *22*, 785-791.

7.   a) C. K. Lee, T. M. Don, W. C. Lai, C. C. Chen, D. J. Lin, L. P. Cheng, *Thin Solid Films* **2008**, *516*, 8399-8407; b) K. E. Gonsalves, L. Merhari, H. P. Wu, Y. Q. Hu, *Adv. Mater.* **2001**, *13*, 703-714.

8.   S. Lee, J. Kwak, Y. Oh, H. S. Lee, *Jpn. J. Appl. Phys.* **2009**, *48*, 1-6.

9.   a) P. T. Wang, J. B. Guo, H. H. Wang, Y. Zhang, J. Wei, *J. Phys. Chem. C* **2009**, *113*, 8118-8123; b) T. Fujigaya, S. Haraguchi, T. Fukumaru, N. Nakashima, *Adv. Mater.* **2008**, *20*, 2151-2155.

10.   W. K. Goertzen, X. Sheng, M. Akinc, M. R. Kessler, *Polym. Eng. Sci.* **2008**, *48*, 875-883.

11.   J. Livage, C. Sanchez, *J. Non-Cryst. Sol.* **1992**, *145*, 11-19.

12.   a) R. A. Caruso, M. Antonietti, *Chem. Mater.* **2001**, *13*, 3272-3282; b) R. J. P. Corriu, D. Leclercq, *Angew. Chem. Int. Ed.* **1996**, *35*, 1420-1436; c) D. R. Uhlmann, G. Teowee, *J. Sol-Gel Sci. Technol.* **1998**, *13*, 153-162.

13.   C. J. Brinker, G. W. Scherer, *Sol-Gel Science: The Physics and Chemistry of Sol-Gel Processing* Academic Press, New-York, **1990**.

14.   Z. Olejniczak, M. Leczka, K. Cholewa-Kowalska, K. Wojtach, M. Rokita, W. Mozgawa, *J. Mol. Struct.* **2005**, *744*, 465-471.

15.   K. G. Sharp, *J. Mater. Chem.* **2005**, *15*, 3812-3820.

16.   a) H. Schmidt, G. Jonschker, S. Goedicke, M. Mennig, *J. Sol-Gel Sci. Technol.* **2000**, *19*, 39-51; b) G. Schottner, *Chem. Mater.* **2001**, *13*, 3422-3435.

17.   a) Y. A. Shchipunov, T. Y. Karpenko, A. V. Krekoten, *Compos. Interf.* **2005**, *11*, 587-607; b) P. W. de Oliveira, C. Becker-Willinger, M. H. Jilavi, *Adv. Eng. Mater.* **2010**, *12*, 349-361.

18.   B. M. Novak, *Adv. Mater.* **1993**, *5*, 422-433.

19.   X. H. Zhang, J. W. Yang, Z. H. Zeng, L. Huang, Y. L. Chen, H. H. Wang, *Polym. Int.* **2006**, *55*, 466-472.

20.   A. Di Gianni, S. Trabelsi, G. Rizza, M. Sangermano, H. Althues, S. Kaskel, B. Voit, *Macromol. Chem. Phys.* **2007**, *208*, 76-86.

21.   a) M. Saric, H. Dietsch, P. Schurtenberger, *Coll. Surf. A* **2006**, *291*, 110-116; b) P. Fabbri, B. Singh, Y. Leterrier, J.-A. E. Månson, M. Messori, F. Pilati, *Surf. Coat. Technol.* **2006**, *200*, 6706-6712.

22.   A. Bandyopadhyay, M. De Sarkar, A. K. Bhowmick, *J. Mater. Sci.* **2006**, *41*, 5981-5993.

23.   M. Sangermano, E. Amerio, P. Epicoco, A. Priola, G. Rizza, G. Malucelli, *Macromol. Mater. Eng.* **2007**, *292*, 634-640.

24.   Y. H. Han, A. Taylor, M. D. Mantle, K. M. Knowles, *J. Non-Cryst. Sol.* **2007**, *353*, 313-320.

25.   P. Hajji, L. David, J. F. Gérard, J. P. Pascault, G. Vigier, *J. Polym. Sci. B Polym. Phys.* **1999**, *37*, 3172-3187.

26.   F. S. Li, S. X. Zhou, L. M. Wu, *J. Appl. Polym. Sci.* **2005**, *98*, 1119-1124.

27.   M. V. Kahraman, M. Kugu, Y. Menceloglu, N. Kayaman-Apohan, A. Gungor, *J. Non-Cryst. Solids* **2006**, *352*, 2143-2151.

28. a) J. H. Zou, W. F. Shi, X. Y. Hong, *Compos. Part A-Appl. Sci.* **2005**, *36*, 631-637; b) J. H. Zou, Y. B. Zhao, W. F. Shi, X. F. Shen, K. M. Nie, *Polym. Adv. Technol.* **2005**, *16*, 55-60.

29. E. Amerio, M. Sangermano, G. Malucelli, A. Priola, B. Voit, *Polymer* **2005**, *46*, 11241-11246.

30. a) A. Di Gianni, R. Bongiovanni, S. Turri, F. Deflorian, G. Malucelli, G. Rizza, *J. Coat. Technol. Res.* **2009**, *6*, 177-185; b) A. Nebioglu, M. D. Soucek, *Eur. Polym. J.* **2007**, *43*, 3325-3336.

31. L. E. Schmidt, D. Schmah, Y. Leterrier, J.-A. E. Månson, *Rheol. Acta* **2007**, *46*, 693-701.

32. V. Geiser, Y. Leterrier, J.-A. E. Månson, *J. Appl. Polym. Sci.* **2009**, *114*, 1954-1963.

33. S. Y. Chou, P. R. Krauss, P. J. Renstrom, *J. Vac. Sci. Technol. B* **1996**, *14*, 4129-4133.

34. V. Geiser, Y. H. Jin, Y. Leterrier, J.-A. E. Månson, *Macromol. Sympos.* **2010**, *296*, 144-153.

35. V. Geiser, Y. Leterrier, J.-A. E. Månson, G. Voirin, M. Wiki, in *Materials Research Society Spring Meeting*, San Francisco, CA, USA **2010**.

36. J. Livage, *Curr. Opin. Solid St. Mater.* **1997**, *2*, 132-138.

37. E. Amerio, M. Sangermano, G. Malucelli, A. Priola, G. Rizza, *Macromol. Mater. Eng.* **2006**, *291*, 1287-1292.

38. C. E. Hoyle, *Calorimetric analysis of photopolymerization*, in *Radiation curing: Science and technology*, S.P. Pappas, Ed., Plenum Press: New York. **1992** p. 57-133.

39. K. S. Anseth, C. M. Wang, C. N. Bowman, *Polymer* **1994**, *35*, 3243-3250.

40. Y. Inoue, Y. Kobatake, *Appl. Sci. Res.* **1958**, *A7*, 314-324.

41.   K. Cottier, M. Wiki, G. Voirin, H. Gao, R. E. Kunz, *Sensor. Actuat. A-Chem.* **2003**, *91*, 241-251.

42.   E. Andrzejewska, *Prog. Polym. Sci.* **2001**, *26*, 605-665.

43.   L. E. Schmidt, Y. Leterrier, D. Schmah, J.-A. E. Månson, D. James, E. Gustavsson, L. S. Svensson, *J. Appl. Polym. Sci.* **2007**, *104*, 2366-2376.

44.   L. Lecamp, B. Youssef, C. Bunel, P. Lebaudy, *Polymer* **1997**, *38*, 6089-6096.

45.   C. N. Bowman, N. A. Peppas, *Macromolecules* **1991**, *24*, 1914-1920.

46.   C. E. Corcione, A. Greco, A. Maffezzoli, *Polymer* **2005**, *46*, 8018-8027.

47.   S. Dalle Vacche, V. Geiser, Y. Leterrier, J.-A. E. Månson, *Polymer* **2010**, *51*, 334-341.

48.   E. Amerio, *PhD Thesis,* Politecnico di Torino, Torino **2008**.

49.   a) Y. Q. Li, H. Ishida, *Macromolecules* **2005**, *38*, 6513-6519; b) D. Fragiadakis, P. Pissis, *J. Non-Cryst. Sol.* **2007**, *353*, 4344-4352.

50.   S. K. Emran, G. R. Newkome, C. D. Weis, J. P. Harmon, *J. Polym. Sci. Pol. Phys.* **1999**, *37*, 2025-2038.

Table of contents entry
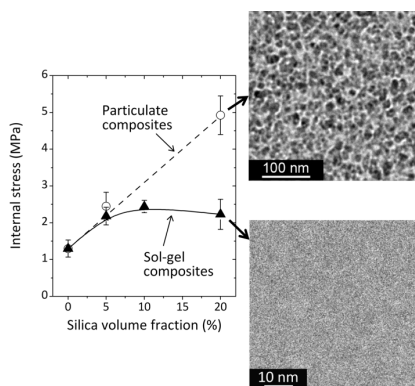
Low-stress hyperbranched polymer/silica nanostructures are produced using either a dual-cure sol-gel and photo-polymerization process or by solvent-assisted mixing with nanoparticles. Optimization of the dual-cure process leads to transparent sol-gel composites with ultrafine structures and internal stress levels as low as 2.5 MPa, a factor of two times lower than particulate nanocomposites. These sol-gel composites are used to accurately replicate nanoscale patterns.